Preprints of the 21st IFAC World Congress (Virtual)
Berlin, Germany, July 12-17, 2020

Model Predictive Controller Development for controlling Actuators of Automated Manual Transmission

Siddharth Lakhera*. Somnath Sengupta**
Vimlendu Singh***

*Advanced Technology Development Centre, Indian Institute of Technology Kharagpur, India,
(e-mail: sid_lakhera@iitkgp.ac.in)
**Advanced Technology Development Centre, Indian Institute of Technology Kharagpur, India
(e-mail: sengupta.s@atdc.iitkgp.ac.in)
*** Mechanical Engineering Department, Indian Institute of Technology Kharagpur, India
(e-mail: vimlendu@iitkgp.ac.in)

Abstract: Automotive transmission technology is evolving rapidly to match up with the growing need of increased power transfer efficiency, tractive demands and powertrain electrification. In this, Automated Manual Transmission (AMT) systems have made their way to the global market as popular choice by automotive industry. AMT applications have grown substantially in Hybrid Electric Vehicles, where hybrid controller decides optimum gear ratio and the gearshift needs to be automated. Advanced model-based predictive techniques for AMT supervisory controllers have allowed complex clutch control, gear shift control and optimal gear-ratio selection. However, the AMT's lower level actuator control is usually done with the help of simple linear controllers like PID. This work aims to evaluate the performance of the AMT system when using a Model Predictive Controller (MPC) for controlling generic AMT actuators. This generic AMT and its control system are modeled and implemented within a HEV vehicle closed loop system model. For gearshift control problem, MPC controller is developed and implemented as actuator controller within the AMT control system framework. A simple PID based actuator controller is also developed to serve as benchmark. The comparative performance of the developed MPC and PID based controllers are evaluated by simulating them during gear-shift operation under a realistic drive cycle. Finally, suitability of MPC for the AMT actuator controller is illustrated through the obtained results.

Keywords: Automated Manual Transmission, Actuators, Gear shift dynamics, Control system design, Model predictive control, Automotive Modeling and Simulation, PID Control.

1. INTRODUCTION

Stricter emission norms are imposing higher efficiency requirement to automotive powertrain technologies. This has resulted in a demand for simple powertrain design with increased functionality. Consequently, the advancements in automotive industry have led to development of highly efficient and innovative AMTs, which deliver comfort of an Automatic Transmission while keeping simplicity of a Manual. Different configurations of AMTs have been identified and extensively used in both solely engine driven as well as electrified powertrain, especially in Parallel Hybrid Electric Vehicles (PHEV). Transmission controls have evolved over time from simple PID based actuation to model based controller with multi-objective optimization performing solving complex problems of launch control, clutch control and gear-shift control which directly and indirectly improve the vehicle efficiency.

Early developments in AMT controls include *Jiang [2009]*, where launch control technique for vehicle with AMT was invented, by calculating clutch slip requirement from driver accelerator pedal position and further converting to torque request. More recent developments in AMT controls have focused on model-based techniques. *Amari [2008]* proposed MPC strategy for controlling vehicle start-up, idle speed and gearshift control. The author developed the system model under different driving conditions of vehicle and formulated (Model Predictive control) MPC to control engine speed and clutch slip in each case. *Ngo [2011]* proposed a predictive control technique for a Parallel HEV that computed gear value which would optimize fuel efficiency over a drive cycle. Clutch control has been widely discussed in literature using predictive control techniques. *Xiaohui [2011]* proposed an MPC strategy to control the clutch during vehicle start-up. A simplified driveline was modeled to optimize clutch slip and torque delivered at wheels. *Li [2016]* implemented detailed DC motor actuated clutch control technique using MPC which used detailed clutch model to estimate resistance torque and compensate for the clutch wear over time. Complete gearshift control was discussed by *Glielmo [2006]*, where different gearshift phases were identified, and decoupled PI controller scheme was implemented for controlling electro-hydraulically actuated clutch. The optimal clutch and transmission input speed trajectories were computed and tracked by different controllers in each discrete gearshift phase. With the evolution of AMT technology, newer designs like discussed by *Tseng*

Copyright lies with the authors

[2015] are making their way into Electric Vehicle market, which is further fuelling the developments in AMT controls.

In most of the literature, MPC is usually considered in the supervisory controller and/or generates speed reference only for engine and clutch. Computational expenses and modelling complexities involved have been the major challenge for the application of MPC for lower level controllers. Most of the actuator level controls are implemented in PID or simple model-based control technique. But increase in electronic controller capabilities and demand for higher control complexity has led us to explore the possibility of using MPC as an actuator level controller and implications of the same. The proposed benefits of using MPC controller for present work at the actuator level is reducing complexity of supervisory controller for actuator control and improved performance of actuator. For the concerned work in this paper, the MPC controller is implemented in a simulation environment while capturing the dynamics of practical system and driving scenarios. The HEV reference model comprising complete vehicle architecture in P2 configuration from Mathworks (*Oshiro [2019]*) is considered. A detailed 5-speed physics-based AMT model capturing the synchronizer dynamics and AMT control system are developed, which replaces the default transmission of the P2 HEV reference model. The MPC based actuator controller is developed and implemented in AMT control system, replacing the PID based actuator controller. The HEV reference model having the detailed AMT model and AMT control system is simulated and the results obtained for both MPC controller and PID based controller are compared. The effects of prediction horizon and sampling rate on the performance of MPC controller and the system response are also analyzed to understand their possible usage for real time applications. Hence, the suitability of MPC controller over PID controller for AMT actuator control is evaluated.

The paper is organized as follow. Section 2 discusses about the AMT system considered in this work. Section 3 describes the development of simple PID controller for use in actuators. Section 4 provides detailed MPC development for AMT. While, section 5 analyses the comparative results of closed loop simulation using both approaches and finally Section 6 provides concluding remarks on the outcome of work.

2. SYSTEM OVERVIEW AND MODELING

The overall AMT system is described in this section. The major components of AMT plant are discussed followed by those of control system.

2.1 System Model

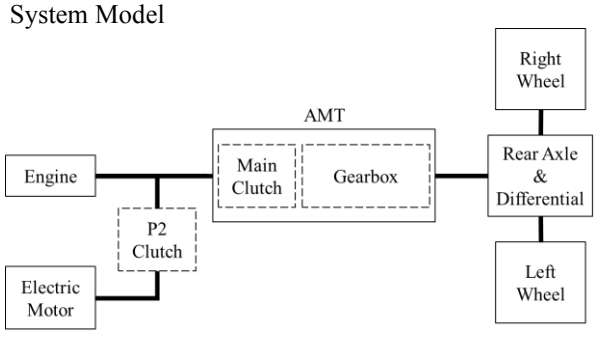

Figure 1. P2HEV vehicle powertrain

The HEV model considered for the work is a closed loop simulation model with the driver as a PID controller for tracking the applied drive cycle. Within the HEV model, the dynamics of Engine, Electric Motor, P2 Clutch, AMT, Differential and Wheels are modeled along with Longitudinal vehicle model for vehicle dynamics. The basic block diagrams of HEV plant model is shown in Figure 1.

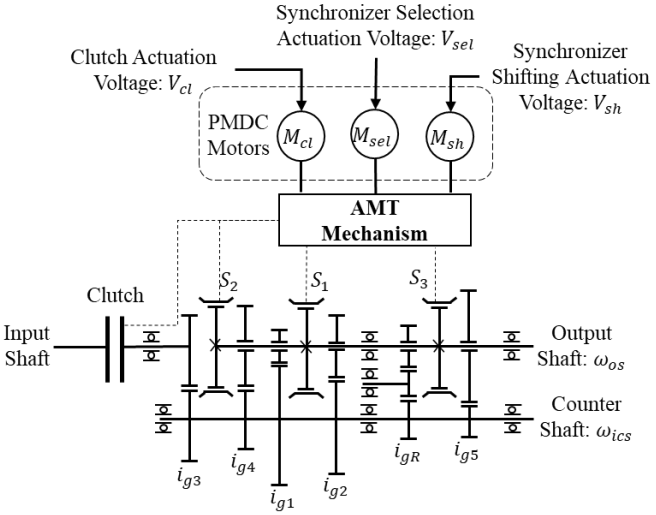

Figure 2. A 5-Speed AMT with mechanism

The AMT considered is a 5-Speed Gearbox with friction clutch driven by an AMT mechanism, shown in Figure 2. The Clutch actuator, synchronizer selection actuator and the synchronizer shifting actuator models are embedded in AMT mechanism; which are responsible for engaging/disengaging the clutch, selection of synchronizer and engaging/disengaging the gearset, respectively. The actuators are PMDC motor, driven by control voltages from AMT controller. In order to keep the modelling generic, the AMT mechanism is considered as a linear mechanical system converting rotational movement of DC motor to linear motion with effective reduction for motor 'm' as $k_{mech,m}$ where 'm' denotes 'cl' for clutch actuation, 'sel' for synchro-selection and 'sh' for synchro shifting motor throughout this paper. Similarly, x_m denotes the linear position of respective actuator. The PMDC actuator equations are given in (1).

$$V_m = i_a R_a + L_a \frac{di_a}{dt} + k_{t,m}\omega_m \quad \text{-(1a)}$$

$$J_m \dot{\omega}_m = k_{t,m} i_a - T_{L,m} \quad \text{-(1b)}$$

$$\dot{x}_m = k_{mech,m}\omega_m \quad \text{-(1c)}$$

The AMT system implementation considers the stick slip kinetic friction model as discussed by *Song [2009]*. The clutch input shafts, output shafts and countershafts are modeled based on their mechanical stiffness and relative damping, represented by (2).

Slip: $$T_{cl} = \mu_{kc} n F_N R_{mean}\, sgn(\omega_c - \omega_{ics}) \quad \text{-(2a)}$$

Stick: $$T_{cl} = \frac{1}{(J_{is}+J_i)}\left\{J_o T_{input} + \omega_c (J_i B_o - J_{is} B_i)\right\} + T_{is,L} \quad \text{-(2b)}$$

$$F_N = k_{spring} x_{cl} \quad \text{-(2c)}$$

$$T_{L,cl} = k_{mech,cl} F_N \quad \text{-(2d)}$$

The load torque on clutch actuator is computed from clutch normal force as in equation (2d). The gearbox has three

identical double-sided synchronizers. The synchronizer is modeled based on the dynamics as described in *Lovas [2006]*, wherein synchronizer's torque is given as in (3a). The k_{sleeve} and k_{sync} are synchronizer related parameters that change based upon synchronizer sleeve position as seen in *Lovas [2006]*. The synchronizer model was validated against data for shift force of a prototype synchronizer obtained from manufacturer. Load torque on synchro-shifting actuator is computed from synchronizer's motion as shown in equation (3c).

$$T_{sync} = k_{sync}\dot{x}_{sh}\left(\omega_{ics} - \frac{\omega_{os}}{i_{gk}}\right) \quad \text{-(3a)}$$

$$F_{load} = B_{sh}\dot{x}_{sh} + F_{fric,sh} + k_{sleeve}\left(\omega_{ics} - \frac{\omega_{os}}{i_{gk}}\right) \quad \text{-(3b)}$$

$$T_{L,sh} = k_{mech,sh}F_{load} \quad \text{-(3c)}$$

The countershaft and output shaft dynamics for AMT are derived based upon the clutch input torque, T_{sync} synchro torque and twisting torque (T_{tor}) between input and output shafts as in (4a) to (4c). The input torque (T_{in}) to the clutch input shaft in (4c) is obtained from engine and/or motor while vehicle load torque ($T_{veh,L}$) in (4c) is obtained from differential as a result of vehicle dynamics.

$$J_{is}\,\dot{\omega}_{ics} = T_{Cl} - \frac{(T_{sync}+T_{tor})}{i_{gk}} \quad \text{-(4a)}$$

$$J_{os}\dot{\omega}_{os} = T_{tor} + T_{sync} - T_{veh,L} \quad \text{-(4b)}$$

$$J_i\dot{\omega}_c = T_{in} - T_{Cl} \quad \text{-(4c)}$$

It is seen from (4a) and (4b), that synchronizer torque as in (3a), on output and counter shafts is nonlinear function of synchro-shifting actuator speed, countershaft shaft (ω_{ics}) and output shaft (ω_{os}) angular velocities. The clutch output speed and countershaft speed are considered same due to permanent unity gear-ratio coupling, hence (J_{is}) is coupled moment of inertia (M.I.) of both the shafts. A list of general symbols used is given in Table 1.

Symbol	Details	Symbol	Details
V_m	Motor input voltage command	k_{spring}	Clutch diaphragm Spring constant
R_a	Motor winding resistance	$F_{fric,sh}$	Synchro sleeve friction
L_a	Motor winding inductance	$T_{is,L}$	Load Torque on Clutch
$k_{t,m}$	Motor Constant	B_{sh}	Drag coefficient
$T_{L,m}$	Motor Load Torque	i_{gk}	AMT kth gear ratio
$T_{em,m}$	Motor Generated Torque	F_N	Clutch Normal Force by actuator
B_i	Rotational damping constant at input	T_{input}	Input torque form Engine/ Motor
J_{csh}	M.I. of Countershaft	R_{mean}	Clutch Mean Radius
ω_c	Clutch input speed	J_i	Clutch input M.I.

Table 1. List of symbols used

2.2 Control System Architecture

A generic AMT controller architecture is shown in Figure 3. The AMT controller consists of AMT supervisory controller and the AMT lower level controller. The supervisory controller is responsible for maintaining the overall transmission state and generating the gearshift command based upon vehicle state and driver inputs.

The lower level controller is responsible for sequencing the actuator operation and providing voltage commands to the AMT mechanism. The sequencing of actuation is based on look-up table specific to AMT mechanism design, which provides the reference positions; $r_{cl}, r_{sh}$and r_{sel} actuator for each gear. The actuator control systems within lower level controller are responsible for generating voltage commands $V_{cl}, V_{sel}$and V_{sh} to track the reference positions. The actuator controller receives actuator position feedbacks; x_{cl}, x_{sh}, x_{sel} and other feedbacks from AMT. A gearshift is executed in the following sequence: Clutch disengagement, synchro-shifting actuator disengages the previous gear, synchro-selection actuator selects new gear-set, synchro-shifting actuator engages new gear and clutch engagement. The actuator controller can be a MPC or a PID controller in this paper. The actuator control problem is essentially a position control problem. It is also required to constrain the voltage commands, actuator positions and actuator speeds to avoid damage and heating of mechanism and actuators.

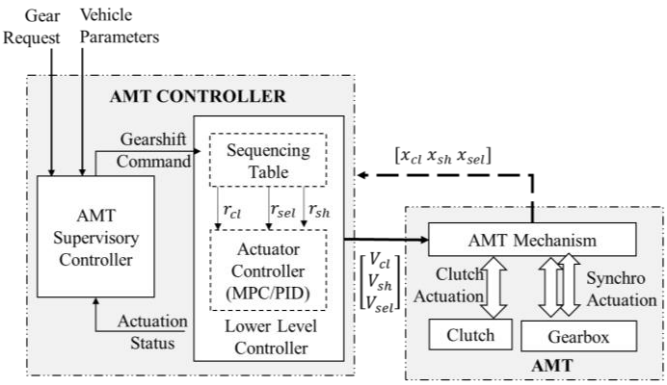

Figure 3. AMT Controller Structure

3. PID CONTROLLER

A simple PID controller implementation scheme is shown in Figure 4, which consists of cascaded PID controllers to control individual actuator. This controller is a four-quadrant PMDC motor controller. The PID controller takes present actuator positions, PMDC motor speeds ($\omega_{cl}, \omega_{sh}, \omega_{sel}$) and motor currents ($i_{cl}, i_{sh}, i_{sel}$) as feedback from AMT and reference positions from supervisory controller. The controller generates voltage commands (V_{cl}, V_{sel}, V_{sh}) to the actuator to track the reference. Thus, 3 PID controllers for each actuator and hence a total of 9 PID controllers are employed for the three actuators.

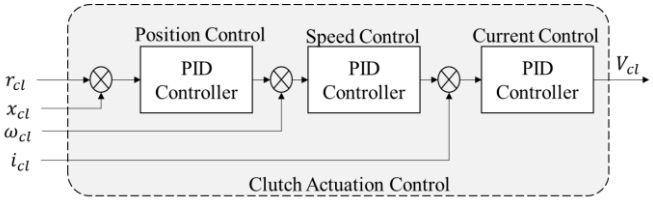

Figure 4. PID Controller Scheme for a sample clutch actuator

4. MPC FORMULATION

The PID controller scheme discussed in previous section requires multiple PID controllers simultaneously operating to address the present multi-input multi-output (MIMO) control problem of AMT control. Within the system, during certain instances it is possible that dynamics of different actuators are coupled, which might result in individual actuator controller operation affecting another actuator, but one set of PIDs will be inherently oblivious to the actions of another set. MPC Controller becomes relevant as an actuator controller, controlling all the actuators simultaneously in a well-coordinated manner since the entire system dynamics are explicitly defined within controller itself.

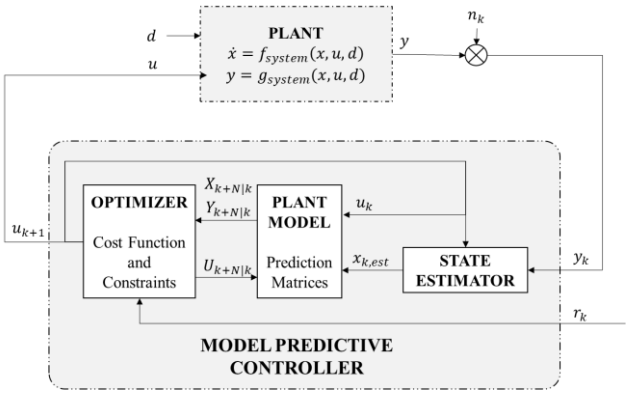

Figure 5. MPC structure overview

The gearshift control using MPC Controller will allow gearshift to be controlled using single control structure. Additionally, it inherently incorporates the constraints and bounds on state variables in the design, as specified by the designer. The MPC structure is shown in Figure 5. Unlike purely error minimizing controller like PID, MPC uses system information to predict control actions until certain prediction horizon (N) during each control step. The computed predicted control inputs are optimized under constraints to calculate optimum system input trajectory within prediction horizon to track output reference. The control input computed for the present instant is applied to the system and the rest are discarded. The accuracy of state feedback computation can be improved by employing a state estimator. The formulation and development stages of MPC for actuator control problem are discussed in subsequent sub-sections.

4.1 Control oriented Model development

A control-oriented system model is developed for implementation in MPC. It is assumed that clutch remains in slipping stage throughout the gearshift stage. The clutch dynamics are hence governed by equation (2a). The output shaft and input shaft dynamics are modelled same as in (4a) and (4b). The synchronizer torque is considered as in (3a). The PMDC actuators' dynamic model as in (1a) is modified to steady state dynamic model as in (5a) for control-oriented model. Corresponding torque equation is given in (5b).

$$J_m\dot{\omega}_m = \frac{V_m k_{t,m} - k_{t,m}^2 \omega_m}{R_a} - T_{L,m} \quad \text{-(5a)}$$

$$T_{em,m} = k_{t,m} i_a = k_{t,m}\left(\frac{V_m - k_{t,m}\omega_m}{R_a}\right) \quad \text{-(5b)}$$

Output shaft load ($T_{L,m}$) is due to the tractive demands of the vehicle. The friction loads on synchro-selection ($F_{fric,sel}$) and synchro-shifting ($F_{fric,sh}$) actuator along with output shaft load ($T_{L,m}$) are considered as exogenous inputs ($\underline{u}_{exo}^T$) to the model. The control-oriented system model structure is a set of nonlinear physics based dynamic equations and is taken from (6a) to (6e), which include the control-oriented plant model characterized by equation (6a). The model of measurement taken from system ($\underline{y}$) are given in (6b). The control inputs ($\underline{u}^T$) which are essentially the input voltages to PMDC motors from controller are given in (6c). The exogenous inputs ($\underline{u}_{exo}^T$) are given in (6d). The system states ($\underline{x}^T$) comprising position and angular speed of actuators are given in (6e).

$$\dot{\underline{x}} = f(\underline{x}, \underline{u}, \underline{u}_{exo}) \quad \text{-(6a)}$$

$$\underline{y} = g(\underline{x}, \underline{u}, \underline{u}_{exo}) = [x_{cl} \quad x_{sel} \quad x_{sl}]^T \quad \text{-(6b)}$$

$$\underline{u}^T = [V_{cl} \quad V_{sel} \quad V_{sl}] \quad \text{-(6c)}$$

$$\underline{u}_{exo}^T = [F_{fric,sel} \quad F_{fric,sh} \quad T_{veh,L}] \quad \text{-(6d)}$$

$$\underline{x}^T = [\omega_{cl} \quad x_{cl} \quad \omega_{sel} \quad x_{sel} \quad \omega_{sh} \quad x_{sh} \quad \omega_{ics} \quad \omega_{os}] \quad \text{-(6e)}$$

4.2 Linearization of State Space

The state space described in Section 4.2 is non-linear in nature. Linear MPC formulation requires linear state-space model for the system. The plant model is linearized at every control step by considering Taylor series expansion of (6a) and (6b) and neglecting all higher order terms. The linearized model is as shown in (7).

$$\dot{\underline{x}} = A.\underline{x} + B_1.\underline{u} + B_2.\underline{u}_{exo} \quad \text{-(7a)}$$

$$\dot{\underline{y}} = C.\underline{x} + D_1.\underline{u} + D_2.\underline{u}_{exo} \quad \text{-(7b)}$$

$$A = \left[\frac{\partial f}{\partial \underline{x}}\right]_{\underline{x}_k, \underline{u}_k, \underline{u}_{exo,k}} \qquad C = \left[\frac{\partial g}{\partial \underline{x}}\right]_{\underline{x}_k, \underline{u}_k, \underline{u}_{exo,k}} \quad \text{-(7c)}$$

$$B_1 = \left[\frac{\partial f}{\partial \underline{u}}\right]_{\underline{x}_k, \underline{u}_k, \underline{u}_{exo,k}} \qquad B_2 = \left[\frac{\partial f}{\partial \underline{u}_{exo}}\right]_{\underline{x}_k, \underline{u}_k, \underline{u}_{exo,k}} \quad \text{-(7d)}$$

$$D_1 = \left[\frac{\partial g}{\partial \underline{u}}\right]_{\underline{x}_k, \underline{u}_k, \underline{u}_{exo,k}} \qquad D_2 = \left[\frac{\partial g}{\partial \underline{u}_{exo}}\right]_{\underline{x}_k, \underline{u}_k, \underline{u}_{exo,k}} \quad \text{-(7e)}$$

$$\left[\frac{\partial f}{\partial \underline{x}}\right]_{\underline{x}_k, \underline{u}_k, \underline{u}_{exo,k}} = \begin{bmatrix} \frac{\partial f_1}{\partial x_1} & \cdots & \frac{\partial f_1}{\partial x_{ns}} \\ \vdots & \ddots & \vdots \\ \frac{\partial f_{ns}}{\partial x_1} & \cdots & \frac{\partial f_{ns}}{\partial x_{ns}} \end{bmatrix} \quad \text{-(7f)}$$

$$\dot{x}_i = f_i(x_1, x_2 \ldots . x_{ns}) \quad \text{-(7g)}$$

The operation $\left[\frac{\partial f}{\partial \underline{x}}\right]_{\underline{x}_k, \underline{u}_k, \underline{u}_{exo,k}}$ denotes Jacobian of function f with respect to each variable of state vector $\underline{x}$ evaluated under $\underline{x}_k, \underline{u}_k$ and $\underline{u}_{exo,k}$ at the k^{th} time instant. The Jacobian matrix is defined as in (7f), where ns is number of state variables and f_i is the state function for i^{th} state x_i as in (7g). A and C are hence Jacobian of $f(\underline{x}, \underline{u}, \underline{u}_{exo})$ and $g(\underline{x}, \underline{u}, \underline{u}_{exo})$ with respect to $\underline{x}$ as in 7(c). B_1 and B_2 are Jacobian of $f(\underline{x}, \underline{u}, \underline{u}_{exo})$ with respect to input vectors $\underline{u}$ and $\underline{u}_{exo}$ as in 7(d). D_1 and D_2 are Jacobian of $g(\underline{x}, \underline{u}, \underline{u}_{exo})$ with respect to input vectors $\underline{u}$ and $\underline{u}_{exo}$ respectively as in 7(e). This linearized state space is therefore obtained using continuous time state space matrices:

A, C, B_1, B_2, D_1, D_2 as in (7a) and (7b). The discrete-time linear state space equations; (8a) and (8b) are obtained by applying Euler's method on the continuous time state space matrices.

$$x_{k+1} = A_k x_k + B_{1,k} u_k + B_{2,k} u_{exo,k} \quad \text{-(8a)}$$
$$y_k = C_k x_k + D_{1,k} u_k + D_{2,k} u_{exo,k} \quad \text{-(8b)}$$

4.3 Prediction Matrices

The linearized state space computed in equation (8a) and (8b), are used to compute the prediction matrices T, S, V, I, H and K given by equation (9a) to (9h). These equations are obtained by iteratively solving the linearized state space equations over set of predicted inputs. $X_{N,P}$, $Y_{N,P}$ and U are set of all predicted states, outputs and control action respectively till $(N\text{-}1)^{\text{th}}$ time step as in (9c) and (9d). $\underline{x}_0$ and u are the state vector and control actions at the present instant, k. The exogenous inputs $\underline{u}_{exo}$ are assumed to be constant over prediction horizon since the frictional loads on actuators and vehicle load on AMT does not vary significantly over prediction horizon.

$$X_{N,P} = T\underline{x}_0 + SU + VU_{exo} \quad \text{-(9a)}$$
$$Y_{N,P} = I\underline{x}_0 + HU + KU_{exo} \quad \text{-(9b)}$$

Where:

$$X_{N,P}{}^T = [\underline{x}_2 \quad \underline{x}_3 \quad \cdots \quad \underline{x}_{N+1}] \quad \text{-(9c)}$$
$$Y^T{}_{N,P} = [Y_1 \quad Y_2 \quad \cdots \quad Y_N] \quad \text{-(9d)}$$
$$U^T = [u_1 \quad u_2 \quad \cdots \quad u_N] \quad \text{-(9e)}$$
$$U_{exo}^T = [u_{exo_1} \quad u_{exo_2} \quad \cdots \quad u_{exo_2}] \quad \text{-(9f)}$$

$$S = \begin{bmatrix} B_1 & 0 & \cdots & 0 \\ AB_1 & B_1 & \ldots & 0 \\ \vdots & \vdots & \ddots & \vdots \\ A^{N-1}B_1 & A^{N-2}B_1 & \cdots & B_1 \end{bmatrix} \quad \text{-(9g)}$$

$$V = \begin{bmatrix} B_2 & 0 & \cdots & 0 \\ AB_2 & B_2 & \ldots & 0 \\ \vdots & \vdots & \ddots & \vdots \\ A^{N-1}B_2 & A^{N-2}B_2 & \cdots & B_2 \end{bmatrix} \quad \text{-(9h)}$$

$$I = CT, H = CS, K = CV \quad \text{-(9i)}$$

4.4 Cost Function Formulation

To obtain the predicted control inputs, the control problem must be formulated as an optimization problem consisting of an objective function and associated constraints. The reference vector to be tracked by system output is given by equation (10a). Assuming that, tracking reference remains the same throughout prediction horizon, the reference vector is computed as in equation (10b).

$$\underline{r} = [r_{cl} \quad r_{sel} \quad r_{sh}]^T \quad \text{-(10a)}$$

$$\underline{R}^T = \left[\underline{r}^T \quad \underline{r}^T \quad \ldots \underline{r}^T\right]_{Nx1}{}^T \quad \text{-(10b)}$$

For each control step, the objective for controller is to minimize the error between reference and output for complete prediction horizon. This control objective is formulated as in equation (11).

$$min: \frac{1}{2}\left(\underline{R} - \underline{Y}\right)^T . \left(\underline{R} - \underline{Y}\right) \quad \text{-(11)}$$

The inequality constraints on voltage command are formulated as in equation (12). The states for actuator speed and position in the state vector must be constrained within upper and lower bounds. The linear state constraints on states over the prediction horizon are given as in (13). These constraints are basically imposed on actuator angular speeds which are a part of system state vector until prediction horizon.

$$M_1 U \leq G_1 \quad \text{-(12)}$$
$$M_{state} X_{N,P} \leq G_{state} \quad \text{-(13)}$$

M_{state} matrix relates the states of predicted state vectors to their respective inequality constraint. These constraints are translated into constraints on predicted input vector U with the help of prediction matrices as in (9a). The final constraints developed are in equation (14a) to (14c).

$$M_2 U \leq G_2 \quad \text{-(14a)}$$

Where:

$$M_2 = M_{state} . S \quad \text{-(14b)}$$
$$G_2 = G_{state} - M_{state} . T - M_{state} . V . U_{exo} \quad \text{-(14c)}$$

Constraints on magnitude of PMDC motor torque are imposed to limit the actuator heating. The PMDC motor torque constraints can be written as in (15). The matrices M_i and M_j relate the torque with input voltage command and actuator motor speed. Using equation (5b), the torque constraints on all three actuators are combined in equation (15-16) to provide torque constraint over the complete prediction horizon. The constraints on state and output vectors ensure that system remains in controllable region of operation.

$$\left(T_{em,m} = M_i \underline{u} - M_j \underline{x}\right) \leq G_{torque} \quad \text{-(15)}$$
$$M_{i,P} U - M_{j,P} X_{N,P} \leq G_{torque,P} \quad \text{-(16)}$$

The prediction state vector $X_{N,P}$is substituted from equation (9a) to obtain constraints on predicted input vector U as in equation (17a) to (17c).

$$M_3 U \leq G_3 \quad \text{-(17a)}$$

Where:

$$M_3 = M_{i,P} - M_{j,P} S \quad \text{-(17b)}$$
$$G_3 = G_{torque,P} + M_{j,P} T + M_{j,P} V U_{exo} \quad \text{-(17c)}$$

The reference tracking control problem formulated in (11) is rearranged to create a quadratic optimization problem with respect to predicted input vector U, shown in equation (18a). Augmenting (12), (14a) and (17a) results in speed, torque and voltage command constraint in terms of linear inequality constraint on predicted input vector U, as shown in (18b).

$$min: \frac{1}{2} U^T E U + F^T U \quad \text{-(18a)}$$

such that

$$MU \leq G \quad \text{-(18b)}$$

Where

$$E = 2H^T H \quad \text{-(18c)}$$
$$F = -2H^T\left(R - I\underline{x}_0 - KU_{exo}\right) \quad \text{-(18d)}$$
$$M^T = [M_1 \quad M_2 \quad M_3] \quad \text{-(18e)}$$
$$G^T = [G_1 \quad G_2 \quad G_3] \quad \text{-(18f)}$$

The optimization problem is solved to obtain the optimal value of U under constraints (18b).

5. IMPLEMENTATION AND RESULTS

The MPC and PID controller are designed and implemented in Matlab/Simulink environment (Matlab 2018a). The AMT model discussed in Section 2.1 and 4 replaces the default AMT in P2HEV Simulink model. The AMT controller within the P2HEV model is basically the AMT supervisory controller in the context of control system architecture discussed in Section 2.2. The MPC and PID controller are modeled as actuator controller in AMT. The simulation is executed in closed loop vehicle with driver under FTP-75 drive cycle. The parameters used in the simulation are listed in Table 2.

The MPC prediction horizon is chosen as 20 based upon computation time and controller rate trade-off. Interior point convex optimization technique is used for solving MPC optimization problem. It is implemented by '*quadprog*' routine from optimization toolbox using Simulink coder extrinsic function call. At time (t = 0s), a gearshift is initiated by the AMT supervisory controller, based upon the drive-cycle requirements. The response of MPC and PID controller to gearshift sequencing in terms of actuator position and command voltage is shown by Figure 6 and 7, respectively. The timings for each stage, position references with suggested time bounds for each controller are summarized in Table 3.

Parameter	Value	Unit
MPC/ PID Controller Rate	1	kHz
MPC prediction horizon	20	steps
Vehicle Mass	1500	Kg
Clutch Actuator Motor Power	400	Watt
Synchro-shift Actuator Motor Power	100	Watt
Synchro-select Actuator Motor Power	40	Watt
All Actuator Motor base speed (before mechanism)	3000	RPM

Table 2. Parameters used in Simulation

From the results it is evident that the MPC performs considerably faster than PID controller. The benefit of using model-based control is realized from actuator position achieved under control by clutch and synchro-selection actuator, as shown in Figure 6(a) and 6(c), where the dynamics remain pretty much constant throughout the gearshift. However, during the synchronizer shifting the MPC's performance particularly during transient response deteriorates due to the change in system and modeled dynamics, as seen in Figure 6(b) at time (t=0.8s) for MPC. The actuator position overshoots 0.5mm higher than PID and takes 0.2s more than PID to settle down to reference. The difference between the control-oriented plant dynamics (within MPC) and detailed AMT model dynamics, introduces considerable error during optimization. In contrast to MPC, the 'k_I' factor in PID allows continuous correction of error, regardless of dynamics change and hence the overshoot is reduced faster than MPC. The voltage commands from MPC are more aggressive due to its ability to compare the system present and reference state. This is evident from Figure 7(a), (b) and (c). During clutch actuation in Figure 7(a), MPC commands maximum voltage at the start of actuation, and predicts the braking of actuator as it reaches near to reference at (t = 0.1s) by reversing polarity of voltage command. PID can be tuned for faster response time by increasing proportionality constant (k_P) but it results in substantial increment in steady-state error. Similar trends are observed in Figure 7(c). MPC's poor performance during synchronizer shifting phase (Figure 6(b) and 7(b)) demonstrates the drawback of using linear MPC for hybrid systems which exhibits both: continuous and discrete event dynamics as observed in synchronizer within AMT.

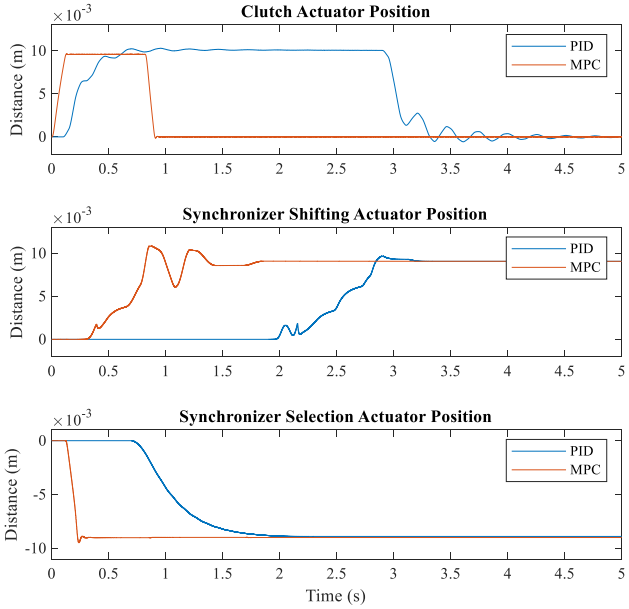

Figure 6. Actuator distances during gearshift (top to bottom) (a) Clutch actuator (b) Synchro-shift actuator (c) Synchro selection actuator

Gearshift Stage	MPC (s)	PID (s)	Dist.(mm)
Clutch disengagement	0.13	0.55	10
Synchronizer Selection	0.12	0.91	9
Synchronizer Shifting	0.42	0.87	9.8
Clutch engagement	0.2	0.95	10

Table 3. Simulation Results obtained: Time spent in different gear-shift phases

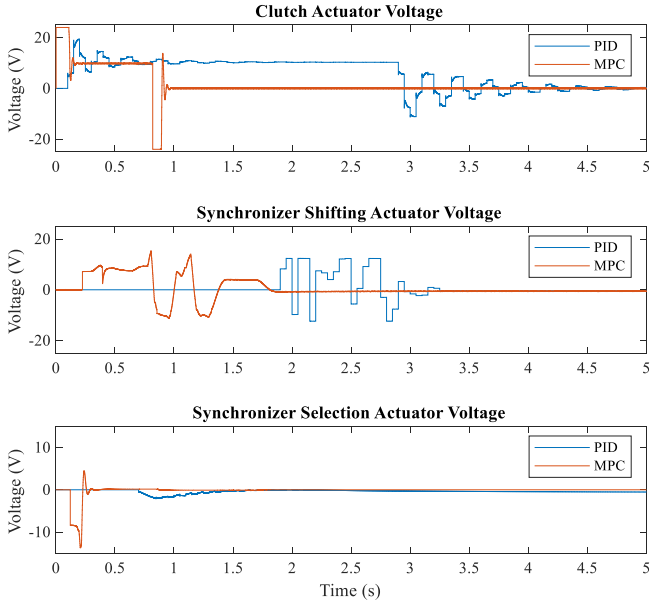

Figure 7. Voltage command from controller: gearshift (top to bottom) (a) Clutch actuator (b) Synchro-shift actuator (c) Synchro selection actuator

The MPC controller is further simulated under multiple control rates and prediction horizon (N). Table 4 summarizes the results obtained in terms of gearshift execution time and steady state root mean square (RMS) error computed for clutch actuator (err_{cl}), selection actuator (err_{sel}) and gear-shifting actuator (err_{sh}).

Rate (Hz)	N	Time (s)	err_{cl} (mm)	err_{sel} (mm)	err_{sh} (mm)
1000	20	0.87	0.12	0.01	0.05
500	15	0.85	0.17	0.05	0.37
100	10	1.18	0.5	0.02	0.18
80	10	1.51	0.48	0.01	0.15

Table 4. Gearshift time and steady state RMS error for different control rates and prediction horizon

At slower control rates, it is observed that steady state RMS error increases for clutch and shifting actuator. The time taken to execute gearshift at 100 Hz is almost 35% more than the time required at 1 kHz. The larger time step at slower control rates leads to loss in fidelity in MPC control oriented model during discretization. Consequently, the accuracy of predicted plant dynamics by MPC is reduced, leading to computation of poorly optimized control inputs. Further, it was observed that upon simulating with controller rates ranging from 200 Hz to 1kHz and prediction horizon ranging from 10 to 30 the gearshift execution times varied between 0.8s to 1.5s. However, among all the results analyzed, the results obtained for control rate 500 Hz and prediction horizon 15 demonstrate acceptable trade-off between execution time and steady state error and might be more suitable for a real-time application than 1 kHz control rate.

6. CONCLUSIONS

PID implementation is simple and straight forward as compared to MPC which requires iterative formulation of prediction matrices and computation intensity. But it is evident from results that MPC performs substantially better than PID controller in terms of tracking reference speed and accuracy. This validates suitability of MPC based actuator controller for AMT. MPC provided a single control structure to solve MIMO control problem under multiple constraints on states and voltage commands. This can prove useful in case of complex actuators used in advanced AMT. However, the MPC performance deteriorated when system underwent dynamics which are unmodeled by control-oriented plant model. This was primarily due to synchronizer dynamics, which are hybrid in nature. In these scenarios, PID performs better than MPC.

A future solution for MPC for such hybrid systems would be to develop a detailed mode-based switching state space which can capture detailed system behaviour as and when the system switches from one state to another. In order to model such detailed dynamics and further improve plant model, state estimators can be used to estimate unknown states. Cost functions for vehicle level performance improvement in terms of reduction in vehicle jerk, driveline vibration and gearshift time can be augmented in the MPC cost function to unify AMT actuator and supervisory control. Following the closed loop simulation results, further work would be implementation of MPC controller on AMT test rig and validation of controller performance in real-time environment.

REFERENCES

Amari, R., Alamir, M. and Tona, P., 2008. Unified MPC strategy for idle-speed control, vehicle start-up and gearing applied to an Automated Manual Transmission. IFAC Proceedings Volumes, 41(2), pp.7079-7085.

Gao, Bingzhao, Lu, Xiaohui, Li, Jun and Chen, Hong. (2011). Model Predictive Control of Gear Shift Process in AMT Trucks. *Proceedings of the ASME Design Engineering Technical Conference*.8.10.1115/DETC2011-47369.

Glielmo, L., Iannelli, L., Vacca, V. and Vasca, F., 2006. Gearshift control for automated manual transmissions. IEEE/ASME transactions on mechatronics, 11(1), pp.17-26.

Jiang, H., Ford Global Technologies LLC, 2009. Automated manual transmission launch control. U.S. Patent 7,630,811.

Li, L., Wang, X., Qi, X., Li, X., Cao, D. and Zhu, Z., 2016. Automatic clutch control based on estimation of resistance torque for AMT. IEEE/ASME Transactions on Mechatronics, 21(6), pp.2682-2693.

Lovas, L., Play, D., Márialigeti, J. and Rigal, J.F., 2006. Mechanical behaviour simulation for synchromesh mechanism improvements. Proceedings of the Institution of Mechanical Engineers, Part D: Journal of Automobile Engineering, 220(7), pp.919-945.

Lu, X., Wang, P., Gao, B. and Chen, H., 2011, May. Model predictive control of AMT clutch during start-up process. In 2011 Chinese Control and Decision Conference (CCDC) (pp. 3204-3209). IEEE.

Ngo, V., Hofman, T., Steinbuch, M. and Serrarens, A., 2011, September. Predictive gear shift control for a parallel hybrid electric vehicle. In 2011 IEEE Vehicle Power and Propulsion Conference (pp. 1-6). IEEE.

Oshiro, K., 2019. HEV Example files for Hybrid Electric Vehicles Video Series (https://www.mathworks.com/matlabcentral/fileexchange/72323-hev-example-files-for-hybrid-electric-vehicles-video-series), MATLAB Central File Exchange. Retrieved November 17, 2019.

Song, X.Y., Sun, Z.X., Yang, X.J. and Zhu, G.M., 2010. Modelling, control, and hardware-in-the-loop simulation of an automated manual transmission. Proceedings of the Institution of Mechanical Engineers, Part D: Journal of Automobile Engineering, 224(2), pp.143-160.

Tseng, C.Y. and Yu, C.H., 2015. Advanced shifting control of synchronizer mechanisms for clutchless automatic manual transmission in an electric vehicle. Mechanism and machine theory, 84, pp.37-56.

Zhao, X., and Li, Z. (2018). Data-Driven Predictive Control Applied to Gear Shifting for Heavy-Duty Vehicles. *Energies*. 11(8), 2139